DYNAMICAL BEHAVIOUR ANALYSIS OF THREE - AXIS MILLING CENTERS

Dan Mihail MARIN[1], Doina MARIN[2], Ramona Cristina VARBAN[3]

Lucrarea prezintă analiza comportării dinamice a unui centru de prelucrare cu arbore principal vertical atât la funcţionarea fără sarcină, cât şi în sarcină. Sunt analizate teoretic şi cercetate experimental modul de comportare al sistemului de avans şi al arborelui principal. Experimentările au fost efectuate pentru a demonstra modul de transmitere a vibraţiilor la diverse elemente componente ale structurii maşinii-unelte şi influenţa acestora asupra prelucrării. Totodată, s-a analizat eroarea traiectoriei liniare de-a lungul unui unghi drept, inconvenient care apare în special la maşinile-unelte cu viteze mari de proces.

The paper presents the dynamic behavior analysis for a vertical machining center during milling process or without load. We have analyzed theoretically and experimentally the behavior of the feed drives systems and spindle. The experimental research shows transmission of vibrations to the mechanical components of the machine tool and theirs influence upon the cutting process. In the same time, we have analyzed the linear motion trajectories containing a square corner, which can be regarded as an important factor to evaluate the performance of high speed machining.

Keywords: ball-screw, spindle, stiffness, feed drive, machine tools, vibrations.

1. Introduction

In the recent years, the machine tools construction sector has been affected by a strong international competition. As a result, companies in NC machine tool sector are under constant pressure to increase both the productivity and machining quality of their products. Increasing both the machining speed and machining quality puts high demands on the dynamic and thermal behavior of the feed systems of modern machine [1].

The flexibility regarding the structure elements has to be taken in consideration for the study of dynamic behavior of machine tools. For this reason, the dynamical model of the axes or of entire machine tools play a very important role for part dimensioning and also for control design [2].

[1] Eng., Research Department, S.C. AEROFINA S.A, Bucharest, Romania
[2] Scientific researcher, Institute of Solid Mechanics – Romanian Academy, Bucharest, Romania
[3] Eng., PhD Student, University POLITEHNICA of Bucharest, e-mail: crissram@yahoo.com

The general way of considering a machine tool as a massive structure leads to high structural stiffness, desired for reducing deformation under the influence of machining forces and static weight of the machine structure and of the work-piece. The structure deflection, which can be regarded as a structural loop deformation, leads to errors at the interface between the tool edge and the work-piece. Stiff machine tool structures tend to transmit vibrations at higher frequencies than compliant (un-stiff) ones [2], [3].

Feed drive systems consist of several subsystems such as force transmission mechanisms, actuators, sensors, controllers and amplifiers. Most of the performed studies are based on the component design methodology, which solely focuses on the design or optimization of each subsystem. However, performance of feed drive systems depends not only upon the characteristics of each subsystem but also upon the interaction between the subsystems. This leads to the conclusion that it is impossible to achieve maximum performance of the feed drive systems through the component design methodology [4], [5].

For these reasons, we have analyzed in this paper a model for feed drive system, analyzing the stiffness, the frequencies, the response of the structure under impact hammer and the dynamic behavior of machine tool during the milling process.

2. Dynamics of the milling process

Two structures contribute to the cutting dynamics: the spindle system and the feeding system. The spindle system (fig. 1) is modeled by a second order system in the X and Y directions.

The equations for tool/spindle system are

$$\begin{aligned} M_{tx}\ddot{X}_t(t) + C_{tx}\dot{X}_t(t) + K_{tx}X_t(t) &= F_x(t) \\ M_{ty}\ddot{Y}_t(t) + C_{ty}\dot{Y}_t(t) + K_{ty}Y_t(t) &= F_y(t) \end{aligned}, \qquad (1, \text{a,b})$$

where: M_t, C_t and K_t represent tool mass, damping and stiffness, respectively; X_t and Y_t are the displacements of the tool in X - and Y - directions, respectively, and $F(t)$ is the cutting force.

The formation of cutting force and the excitation of the machine structure by the cutting force contribute to the cutting dynamics. The dynamic model of the milling cutter used in this paper is assumed to be a system with two modes of vibration in two perpendicular directions, X and Y, while the feed direction is along the X-axis.

The milling system under consideration is shown in fig. 1, where the X-Y coordinate system is fixed with respect to the machine tool structure and its axes are aligned with the principal modes of oscillation. This is a common

characteristic of the spindle tool assembly, which is the most flexible part of a typical milling machine. The milling cutter has *n* teeth, which are assumed to be equally spaced.

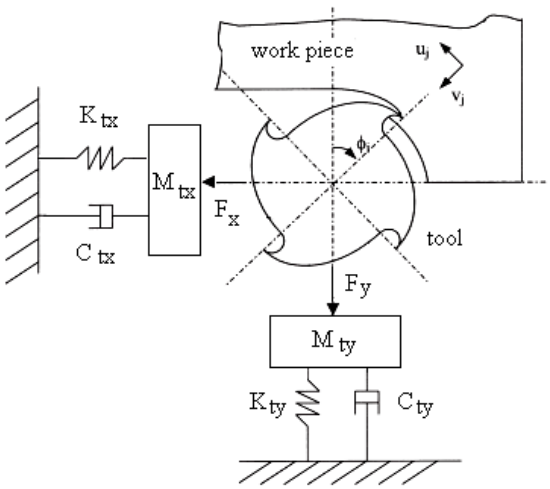

Fig. 1. Dynamic model for spindle system.

The dynamics of the milling system are given by equations (1, a,b). In order to express the cutting force $F(t)$ the rotating coordinate system $u_j - v_j$ is used. Referring to the system, any tooth of the milling cutter can be view as a single point cutting tool, thus the predictive machining theory established for turning can now be used. For tooth number (j), which is the instantaneous angular immersion ϕ_j, measured clockwise from the negative Y-axis at a particular instant, the milling force components, P_{1j}, P_{2j}, P_{3j}, which are oriented in the tangential, radial and axial directions respectively, are calculated from the corresponding chip loads, cutting conditions, and tool geometry by using the single-point cutter mechanics as mentioned above.

The total cutting forces of the cutter can be determined using the following equations

$$\begin{cases} F_x(t) = \sum_{j=0}^{n-1} F_{xj} = \sum_{j=0}^{n-1} (P_{1j}\cos\phi_j + P_{2j}\sin\phi_j) \\ F_y(t) = \sum_{j=0}^{n-1} F_{yj} = \sum_{j=0}^{n-1} (-P_{1j}\sin\phi_j + P_{2j}\cos\phi_j) \end{cases} \tag{2}$$

where the immersion angle ϕ_j varies with time as $\phi_j(t) = \Omega t$; F_{xj} and F_{yj} are the components of the cutting force applied on the j th tooth.

3. The analysis of feed drive system

Machine tools designs vary considerably, while the mechanical configuration of their feed drive system is largely standardized. In almost all cases, the recirculation ball-screw has established itself as the solution for converting the rotary motion of the servomotor into linear slide motion of the tool. The ball-screw is normally fixed in axial direction at only one end, with a preloaded angular contact ball bearing, which takes up the axial forces of the slide. The servomotor and the ball-screw drive are usually directly coupled. Toothed-belt drives are also widely used to achieve a compact design and better adapt to speed.

The first step in any machine tool design process is to establish a simplified scheme of its mechanical structure. In this regard, the main components of feed drive system are presented in fig. 2,*a* and the equivalent model for axial stiffness looks like in fig. 2,*b*.

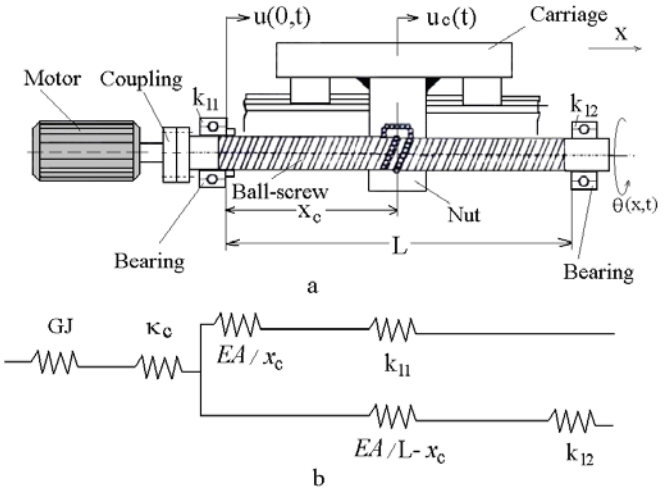

Fig. 2. Feed drive system:
a) the structural scheme; *b*) equivalent model for axial stiffness.

The motion equations are

$$E\ddot{u}(x,\omega)+\rho\omega^2 u(x,\omega)=0,\ G\ddot{\theta}(x,\omega)+\rho\omega^2\theta(x,\omega)=0 \qquad (3,\text{a,b})$$

where $u(x,t)$ is the longitudinal displacement, $\theta(x,t)$ the angle of rotation of the screw, ρ is the density, E the ball-screw Young' modulus, G the ball-screw shear modulus and ω the frequency.

The boundary conditions are:

a) Conditions at the ball-screw for $x = 0$ and $x = L$ (the ends of screw)

$$EA\dot{u}(0,\omega) = k_{l1}u(0,\omega),\ EA\dot{u}(L,\omega) = k_{l2}u(L,\omega) \tag{4, a,b}$$

$$GJ\dot{\theta}(0,\omega) = k_c\left[\theta(0,\omega) - \theta_m(\omega)\right] \tag{5}$$

b) Conditions of the nut

$$u_c(\omega) = u(x_c,\omega) + \theta(x_c,\omega)\frac{p}{2\pi} \tag{6}$$

c) Conditions at the motor and carriage

$$\left(-\omega^2 J_m + j\omega C_m + \kappa_c\right)\theta_m(\omega) = M_m + \kappa_c\theta(0,\omega) \tag{7}$$

where k_{l1} is the combined axial stiffness of the thrust bearing ant the housing, k_{l2} - the stiffness at the end farthest from the motor, κ_c - the torsion stiffness of the coupling between the motor and screw, k_p - the axial stiffness of the nut, d - the ball-screw diameter, p - the ball-screw lead, L - the ball-screw length between bearing supports, J - the second polar moment of the cross-section of the screw, J_m - the moment of inertia of the motor, m_m - the mass of the carriage, C_m - the viscous damping constant of the motor.

The forces and displacements are

$$F = k_t\left[u_c(\omega) - \theta_m(\omega)\frac{p}{2\pi}\right] \tag{8}$$

where k_t is the total stiffness, while the inertia of the system is neglected.

Making use of equation (5), we write the angular displacements at $x = 0$ and x_c in terms of $u_c(\omega)$ and $\theta_m(\omega)$ as

$$\begin{pmatrix}\theta(0,\omega) - \theta_m(\omega)\\ \theta(x_c,\omega) - \theta_m(\omega)\end{pmatrix} = \begin{pmatrix}1/\kappa_c\\ 1/\kappa_{tc}\end{pmatrix}\frac{k_t p}{2\pi}\left[u_c(\omega) - \theta_m(\omega)\frac{p}{2\pi}\right] \tag{9}$$

where $\kappa_{tc} = \dfrac{1}{\kappa_c} + \dfrac{x_c}{GJ}$

Making use of (4, a,b) we can write the stiffness of the screw and of the thrust bearings to the left and right of the nut at moment $x = x_c$

$$k_1 = \left(\frac{x_c}{EA} + \frac{1}{k_{l1}} \right)^{-1} \quad k_2 = \left(\frac{L - x_c}{EA} + \frac{1}{k_{l2}} \right)^{-1} \tag{10, a,b}$$

The total force F given by equation (8) is divided among the portions of the screw to the left and to the right of the nut. We write the longitudinal displacements as

$$\begin{pmatrix} u(0,\omega) \\ u(x_c,\omega) \\ u(L,\omega) \end{pmatrix} = \begin{pmatrix} k_2 / k_{l1} \\ 1 \\ k_1 / k_{l2} \end{pmatrix} \frac{k_t}{k_1 + k_2} \left[u_c(\omega) - \theta_m(\omega) \frac{p}{2\pi} \right] \tag{11}$$

Finally, we combine the second row of equation (9), the middle row of equation (11), and equation (8) to obtain an expression for the total stiffness k_t

$$k_t = \left[\frac{1}{k_1 + k_2} + \frac{1}{k_p} + \left(\frac{p}{2\pi} \right)^2 \left(\frac{1}{\kappa_c} + \frac{x_c}{GJ} \right) \right]^{-1} \tag{12}$$

We can analyze now the stiffness of feed drive systems for a vertical milling center according to the characteristics of the machine tool presented in table 1.

Table 1

Parameters of feed drive system

Parameters	Simbol	Dimensions
Ball-screw diameter	d	40 mm
Ball-screw lead	p	10 mm
Ball-screw length between bearing supports for X axis	L	1100 mm
Ball-screw length between bearing supports for Y axis	L	700 mm
Ball-nut stiffness	k_p	720 N/μm
Bearing stiffness	$k_{l1}=k_{l2}$	1500 N/μm
Torsional stiffness of coupling	κ_c	625 Nm
Motor inertia	Jm	$12x10^{-5}$ kg m^2
Carriage mass	m_c	1500 kg
Support mass	m_c	1000 kg
Density of ball-screw	ρ	7,8 kg/dm^3
Ball-screw Young's modulus	E	$2{,}1 \cdot 10^6$ daN/cm^2
Ball-screw shear modulus	G	$8{,}1 \cdot 10^6$ N/cm^2

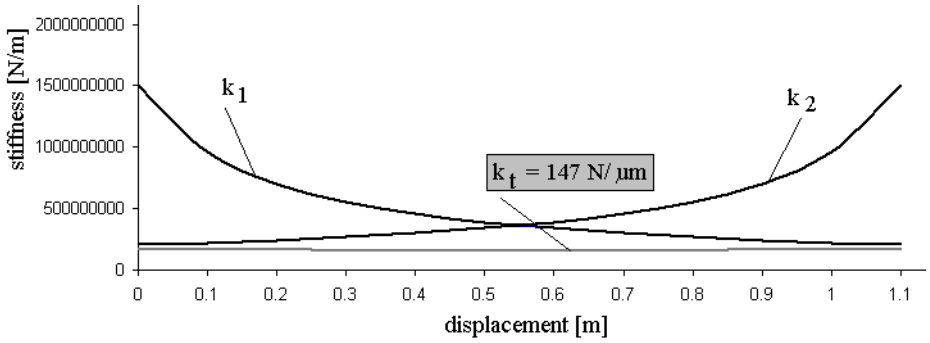

Fig. 3. The stiffness of a milling center for *X* axis.

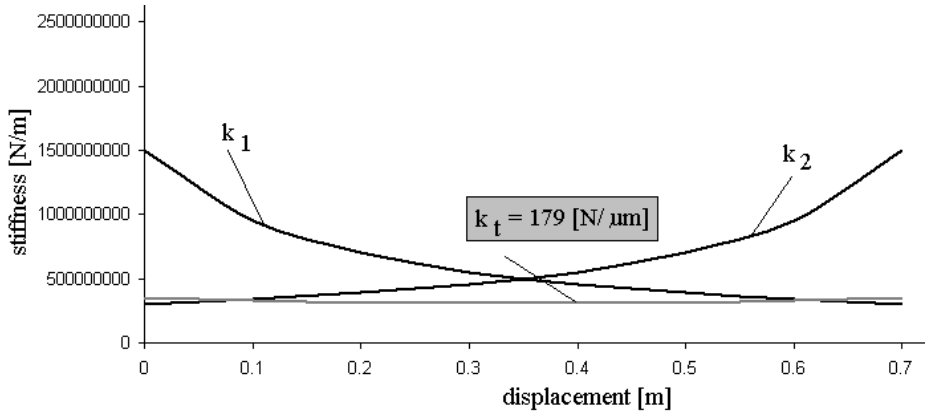

Fig. 4. The stiffness of a milling center for *Y* axis.

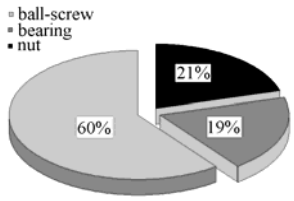

Fig. 5. The influence of the component elements for *X* axis of milling center.

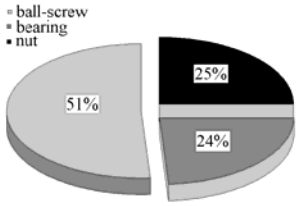

Fig. 6. The influence of the component elements for *Y* axis of milling center.

In fig. 3 and fig. 4 we show the total stiffness for *X* axis, respectively *Y* axis of three-axis milling center. The total stiffness in the second case increases because the length of the ball-screw between bearing supports is smaller than in the first case (see table 1).

The influence of the component elements for feed drive system, to the middle of the ball-screw, upon total stiffness is presented in fig. 5 for *X* axis and

in fig. 6 for the *Y* axis. We observe that the influence of the ball-screw is bigger than the influence of the nut and the bearings.

With the parameters in table 1 and equations (10, a,b) and (12) we have calculated the frequency along the length of the ball-screw for the axis participating into interpolation, axes *X* and *Y* in this situation, represented in table 2. The conclusion is that for *X* axis the frequencies are lower because the moving mass is higher, and for the *Y* axis the frequency is bigger, because the total stiffness is higher due to the shortness of the ball-screw.

Table 2

Frequencies variations owing to total stiffness of the feed drive system

Displacement [m]	Frequency of *X* axis [Hz]	Frequency of *Y* axis [Hz]
0	52.92983	70.12653
0.1	51.819	68.68987
0.2	50.97898	67.77969
0.3	50.37508	67.33788
0.4	49.98417	67.33772
0.5	49.79205	67.77921
0.6	49.79195	68.68903
0.7	49.98388	70.12528
0.8	50.37459	
0.9	50.97827	
1	51.81804	
1.1	52.92983	

4. Experimental set up

The experimental system (fig. 7) used in this study is built of: the computer with the acquisition board DAQ-500, the amplifier model 480B21 and three accelerometers of type PCB 353B33. The sampling frequency is 1200 Hz per channel.

Work-pieces are made of aluminum alloy; the cutter is a three-edge, high-speed steel milling tool, with a diameter of 50 mm. The trajectories are circular and linear with continuous path. Test piece for performance tests of continuous path controlled milling machines is the well-known work piece NAS 913, presenting a circular contour and a square.

Cutting conditions were set as: spindle speed 710 rpm, feed rate 150 mm/min for heavy milling, the cutting depth 10 mm.

In order to examine the effects of feed rate and spindle, the rectangular and circular trajectory are machined with different feed rates and spindle speeds, with

accelerometers mounted in different places: on the table, on the work piece device and on the housing spindle.

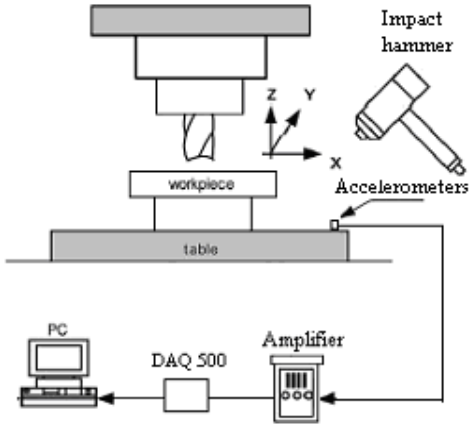

Fig. 7. Experimental set up.

5. System analysis

An impact hammer excited the table and the signals from accelerometers were collected and analyzed. This type of measurement is used to make a modal model of the structure, which can than be used to predict the behavior of the structure under given circumstances. The response of the system measured in the same point on the three directions (*X*, *Y*, *Z*) of the machine tool are presented in fig. 8. In this case, the accelerometers are fitted on the table. Using FFT analyses, the frequency response of the table system was illustrate in fig.9.

The peak of the frequency is at 52 Hz. A higher harmonic comes to 156 Hz. Besides the eigenvalue frequency other two frequencies can be seen at 22 Hz and 33 Hz.

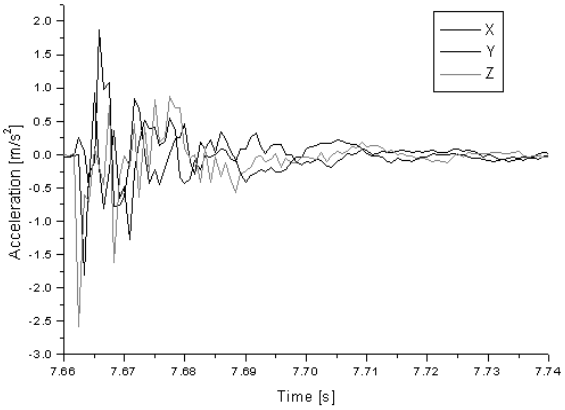

Fig. 8**.** Shock response at impact hammer.

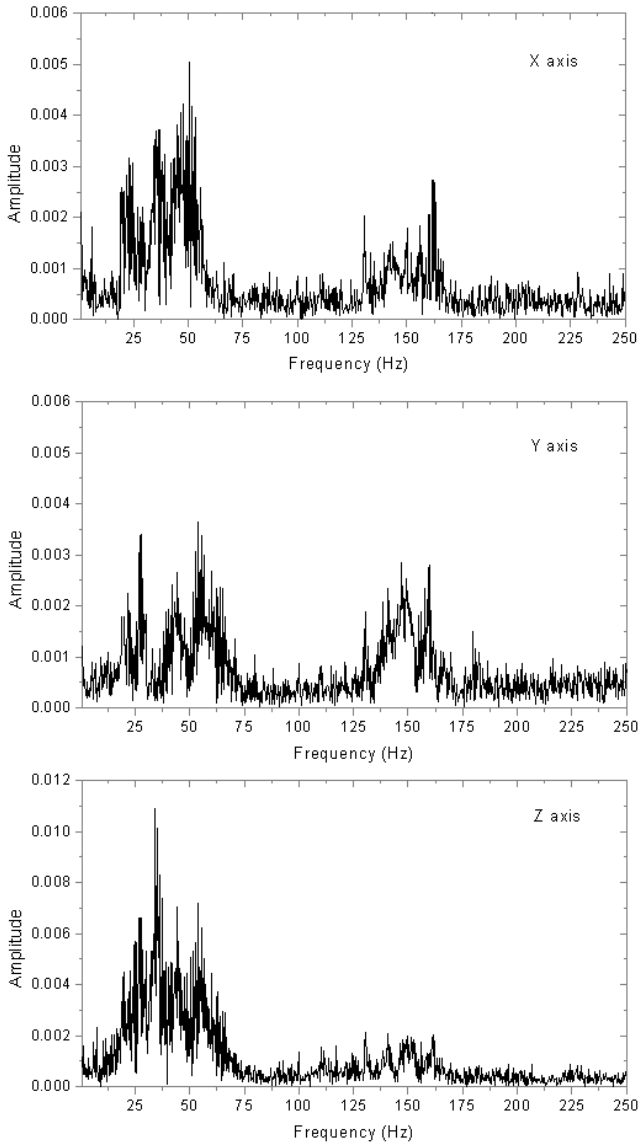

Fig. 9. Amplitude-frequency characteristics.

6. Experiments with no load applied

Experiments are made on a vertical milling machine with accelerometers fitted on the table or on the cross-tool carriage, with moving carriage along the working stroke. The carriage was driven forward and backward with no load applied on *X* and *Y* axes.

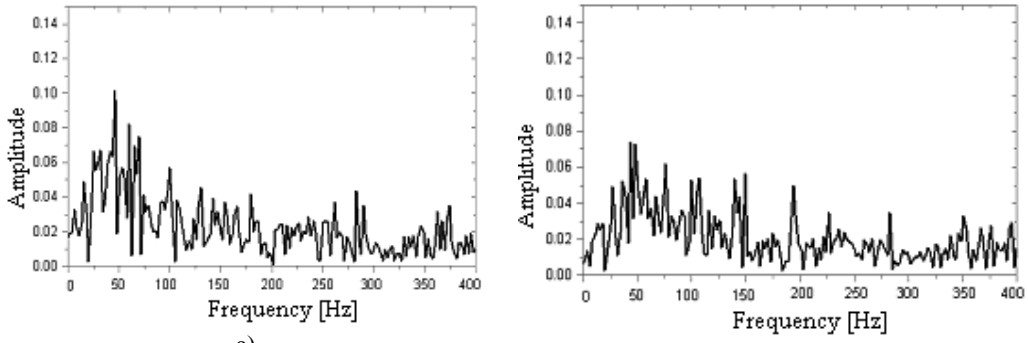

Fig. 10. Amplitude-frequencies characteristics for *X* axis moving table with feed 300 mm/min: a) forward direction; b) backward direction.

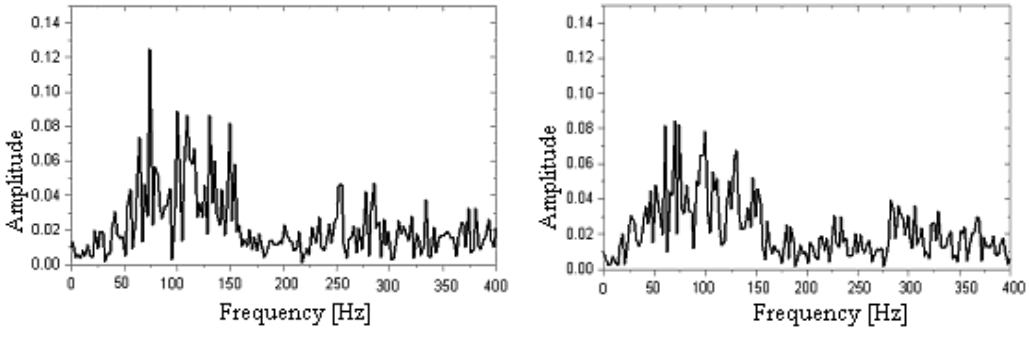

Fig. 11. Amplitude-frequencies characteristics for *Y* axis moving carriage with feed 300 mm/min: a) forward direction; b) backward direction.

Amplitude-frequencies characteristics during carriage motion along the *X* axis with a feed rate of 300 mm/min is presented in fig. 10, and for the *Y* axis ~~is presented~~ in fig. 11. Comparing the experimental results with the theoretical ones (see chapter 3) we observe that the values of the frequencies are close. On the other hand, comparing the forward and backward motion, the amplitudes increase or decrease when the direction is changed because the stiffness of the mechanical components of feed drive system is varying due to the pre-loaded.

With accelerometers mounted on the housing spindle, with spindle shaft out to 1/3 of his length, vibrations were measured for different speeds. The position of the axes of the machine tool during the tests is presented in fig. 12. Figure 13 shows the vibrations on axis *X*, *Y*, *Z* for a spindle speed of 710 rpm. In this figure, we can observe the accelerating/braking and constant parts of the

motion under no-load conditions. The vibrations are lower in the Z direction, because the spindle is situated

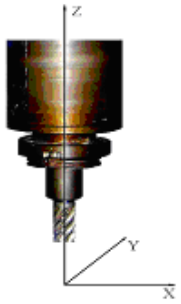

Fig. 12. Axes position during measurement.

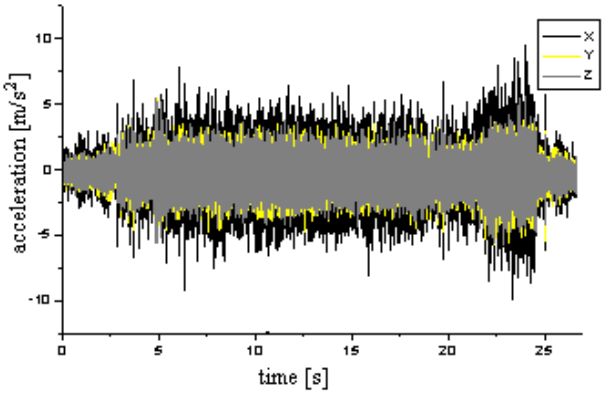

Fig. 13. Vibrations during spindle rotation with 710 rpm.

in a vertical position and the unbalance caused by an imprecision assembly and execution are manifested in *X* and *Y* directions only.

8. Experimental results during the milling process

The circular trajectory is machined with a feed rate of 150 mm/min and a spindle speed of 710 rpm, with accelerometers mounted on the work-piece device (fig. 14) and on the housing spindle (fig. 15). Comparing these figures, we have observed that the accelerations on the *X* and *Y* axes (participating to the interpolation) are almost equally and on the Z axis are two-times bigger or more, the cause residing in the cutting efforts during peripheral milling.

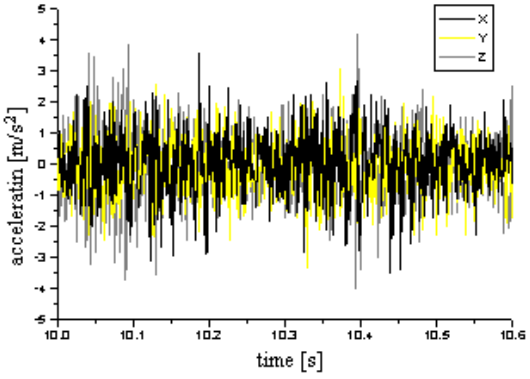

Fig. 14. Vibro-records during the cutting process with accelerometers mounted on the workpiece device.

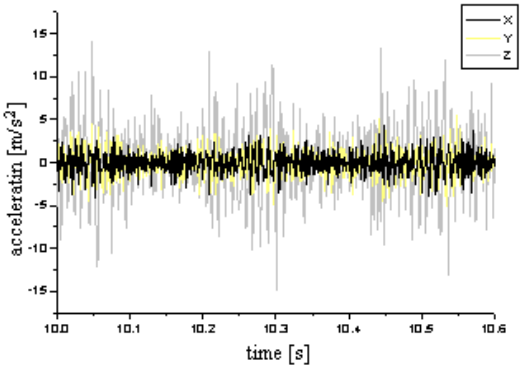

Fig. 15. Vibro-records during the cutting process with accelerometers mounted on the housing spindle.

Linear motion trajectories containing a square corner, during the roughing mill with feed rate 180 mm/min and spindle speed 710 rpm have been analyzed in this paper. For NC machine tools, during the milling process of a continuous path, the tool is positioned tangent to the trajectory (fig. 14). Near the corner, from vibrations diagram presented in fig. 15, it can be observed the decrease of the acceleration on the axes participating to the interpolation, and acceleration increasing when the tool re-enters the semi-finished material again.

On the other hand, while approaching the corner, the speed is reduced along the first linear motion. With a little delay, the second linear motion starts.

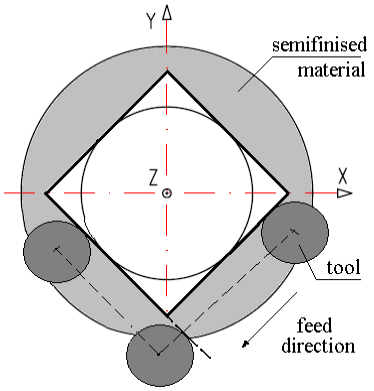

Fig. 14. Tool trajectory in semi-finished material.

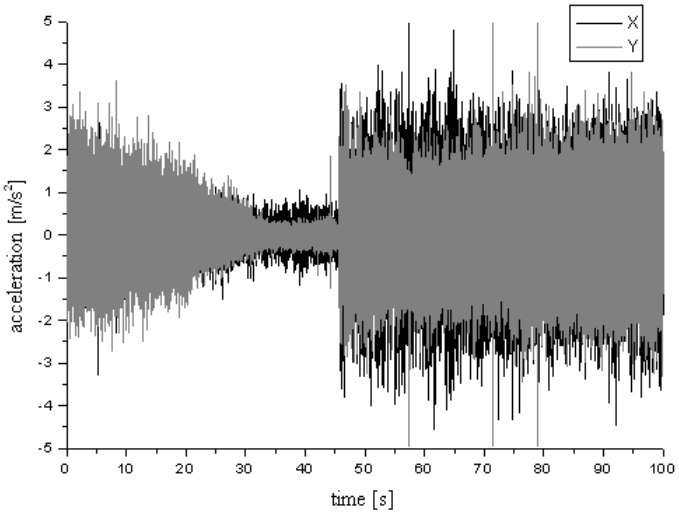

Fig. 15. Vibrations on *X* and *Y* axes during heavy milling.

Because of the inertia of the driving system, increasing the speed to a specified value for the second motion and reducing the speed to zero for the first motion instantaneously are impossible. Therefore, if no dwell between both linear movements has been specified, there is an overlap between the speed reducing process of the first motion and the speed increasing process of the second motion around the corner. As a result, the overlap effect caused the corner error. In other words, in order to obtain a sharp shape, it is necessary to specify a dwell action at the corner in NC contour manufacturing with a high feed rate. The new generation of machine tools has specials functions in their NC programs (for example G 61 and G 62) for correcting the corner error.

9. Conclusions

The paper has investigated all three axes of a milling center. During the movement without load, on the *X* and *Y* axis, we have observed that acceleration amplitudes increase or decrease when the direction of feeding is changed because the stiffness of the mechanical components of feed drive system are varying with the pre-loaded. The same fact is happening during the cutting process because the values and directions of the cutting forces are changed. On the *Z* direction, the acceleration is bigger because during peripheral milling the cutting efforts increase in this direction.

Feed drive errors were evaluated along a square corner path. The experimental results verify that the cause of corner errors in contour manufacturing is due to the increase and the reduction in feed speed near the connection position between two linear motions to form the corner.

R E F E R E N C E S

[1] *C. L. Chen*, *M. J. Jang, K. C. Lin,* Modeling and high-precision control of a ball-screw-driven stage, Precision Engineering, **vol. 28**, 2004, pp.483-495

[2] *F. Stratulat, F. Ionescu, G. Constantin,* Dynamic evaluation of a liniar axis in milling using modeling and simulation environment, Proceedings of International Conference on Manufacturing Systems – ICMaS, Editura Academiei, ISSN 1842-3183, Bucureşti, 2007, pp. 99-104

[3] *C. E. Eisinger-Borcia, D. Marin, E. M. Videa,* Computer-aided model of the dynamic behavior of the feed drive systems, Proceedings of the 9th WSEAS International Conference on Automation and Information, Published by WSEAS Press, ISBN 978-960-6766-77-0, ISSN 1790-5117, Bucureşti, 2008, pp. 103-109

[4] *K. K. Varanasi, S. A. Nayfeh,* The dynamics of lead-screw drives: Low-order modeling and experiments, Journal of Dynamic Systems, Measurement, and Control, Transactions of the ASME, **vol. 126**, 2004, pp. 388-396

[5] *M. S. Kim, S. C. Chung,* A systematic approach to design high-performance feed drive systems, International Journal of Machine Tools & Manufacture, **vol. 45**, 2005, pp. 1421-1435